JOURNAL OF COMPUTATIONAL PHYSICS **146,** 82–104 (1998)
ARTICLE NO. CP986060

A General Class of Commutative Filters for LES in Complex Geometries

Oleg V. Vasilyev, Thomas S. Lund, and Parviz Moin

Center for Turbulence Research, Stanford University, Stanford, California 94305

Received July 31, 1997; revised July 12, 1998

A class of filters for large eddy simulations of turbulent inhomogeneous flows is presented. A general set of rules for constructing discrete filters in complex geometry is given and examples of such filters are presented. With these filters the commutation error between numerical differentiation and filtering can be made arbitrarily small, allowing for derivation of a consistent set of equations for the large scale field. The application of such filters for explicit filtering in large eddy simulations and the issue of boundary conditions for the filtered field are also discussed.

I. INTRODUCTION

In large eddy simulation (LES) of turbulent flows the dynamics of the large-scale structures are computed, while the effect of the small-scale turbulence is modeled using a subgrid-scale (SGS) model. The differential equations describing the space-time evolution of the large-scale structures are obtained from the Navier–Stokes equations by applying a low-pass filter. In order for the resulting LES equations to have the same structure as the Navier–Stokes equations, the differentiation and filtering operations must commute. In inhomogeneous turbulent flows, the minimum size of eddies that need to be resolved is different in different regions of the flow. Thus the filtering operation should be performed with a variable filter width. In general, filtering and differentiation do not commute when the filter width is nonuniform in space.

The problem of noncommutation of differentiation and filtering with nonuniform filter widths was studied by Ghosal and Moin [1], who proposed a new class of filters for which the commutation error could be obtained in closed form. The application of this filter to the Navier–Stokes equations introduces additional terms (due to commutation error) which are of second order in the filter width. Ghosal and Moin suggested that the leading correction term be retained if high-order numerical schemes are used to discretize the LES equations. This procedure involves additional numerical complexities which can be avoided by using filters with specific properties which we will discuss in this paper. Van der Ven [2]

0021-9991/98 $25.00

constructed a family of filters which commute with differentiation up to any given order in the filter width; however, this approach is limited to a specific choice of filters and does not address the issue of additional boundary terms that would arise in finite domains.

Due to the lack of a straightforward and robust filtering procedure for inhomogeneous flows, most large eddy simulations performed to date have not made use of explicit filters. The nearly universal approach for LES in complex geometries is to argue that the finite support of the computational mesh together with the low-pass characteristics of the discrete differencing operators effectively act as a filter. This procedure will be referred to as implicit filtering since an explicit filtering operation never appears in the solution procedure. Although the technique of implicit filtering has been used extensively in the past, there are several compelling reasons to adopt a more systematic approach. Foremost among these is the issue of consistency. While it is true that discrete derivative operators have a low-pass filtering effect, *the associated filter acts only in the one spatial direction in which the derivative is taken.* This fact implies that each term in the Navier–Stokes equations is acted on by a distinct one-dimensional filter, and thus there is no way to derive the discrete equations through the application of a single three-dimensional filter. Considering this ambiguity in the definition of the filter, it is nearly impossible to make detailed comparisons of LES results with filtered experimental data. In the same vein it is not possible to calculate the Leonard term [3] that appears as a computable portion in the decomposition of the subgrid-scale stress.

The second significant limitation of the implicit filtering approach is the inability to control numerical error. Without an explicit filter, there is no direct control in the energy in the high-frequency portion of the spectrum. Significant energy in this portion of the spectrum coupled with the nonlinearaties in the Navier–Stokes equations can produce significant aliasing error. Furthermore, all discrete derivative operators become rather inaccurate for high-frequency solution components, and this error interferes with the dynamics of the small-scale eddies. This error can be particularly harmful [4] when the dynamic model [5,6] is used since it relies entirely on information contained in the smallest resolved scales. In addition, it is difficult to define the test to primary filter ratio which is needed as an input to the dynamic procedure.

The difficulties associated with the implicit filtering approach can be alleviated by performing an explicit filtering operation as an integral part of the solution process. By damping the energy in the high-frequency portion of the spectrum it is possible to reduce or eliminate the various sources of numerical error that dominate this frequency range [7]. Explicit filtering reduces the effective resolution of the simulation, but allows the filter size to be chosen independently of the mesh spacing. Furthermore the various sources of numerical error that would otherwise enter the stresses sampled in the dynamic model can be controlled, which can ultimately result in a more accurate estimate for the subgrid-scale model coefficient. Finally, the shape of the filter is known exactly, which facilitates comparison with experimental data and the ability to compute the Leonard term.

In addition, explicit filtering provides a means of reducing the various sources of numerical error that become most severe for length scales on the order of the mesh size. By damping the high-frequency portion of the solution, it is possible to control the adverse effects of numerical error. In particular, if the filter width is held fixed as the mesh is refined, the velocity field will converge to the true solution to LES equations. This should be contrasted with the conventional approach, where the mesh is refined without the use of an explicit filter. In the latter case, additional length scales are added each time the mesh is

refined, and thus the process converges to a direct numerical simulation (DNS) rather than a LES. The increase in the number of degrees of freedom as the mesh is refined also makes it difficult to distinguish between the effects of reduced numerical error and the increase in the range of resolved length scales. In short, the use of an explicit filter allows a means of both assessing and minimizing the effects of numerical error in practical simulations.

In order to realize the benefits of an explicit filter, it is necessary to develop robust and straightforward discrete filtering operators that commute with numerical differentiation. As mentioned above, the earlier works in this area either required adding corrective terms to the filtered Navier–Stokes equations or required the use of a restricted class of filters that could not account properly for nonperiodic boundaries. The objective of this work is to develop a general theory of discrete filtering in arbitrary complex geometry and to supply a set of rules for constructing discrete filters that commute with differentiation to the desired order.

The paper is organized as follows. In Section II we introduce a general class of variable-width filters that commute with differentiation to any specified power of the mesh spacing. The issue of boundary conditions for the filtered field is discussed there as well. The theory of constructing consistent discrete filters with commutative properties is presented in Section III. Finally, in Section IV we demonstrate the application of discrete filters for consistent explicit filtering in large eddy simulations.

II. COMMUTATION ERROR OF FILTERING AND DIFFERENTIATION OPERATIONS AND BOUNDARY CONDITIONS

Consider a one-dimensional field $\psi(x)$ defined in a finite or infinite domain $[a, b]$. Let $f(x)$ be a monotonic differentiable function which defines the mapping from the domain $[a, b]$ into the domain $[\alpha, \beta]$, i.e., $\xi = f(x)$. $f(x)$ can be associated with mapping of the nonuniform computational grid in the domain $[a, b]$ to a uniform grid of spacing Δ, where the nonuniform grid spacing is given by $h(x) = \Delta / f'(x)$.

Let $x = F(\xi)$ be the inverse mapping $(F(f(x)) = x)$. The filtering operation is defined in analogous way as in [1]. Given an arbitrary function $\psi(x)$ we obtain the new function $\phi(\xi) = \psi(F(\xi))$ defined on the interval $[\alpha, \beta]$. The function $\phi(\xi)$ is then filtered using the definition

$$\bar{\phi}(\xi) = \frac{1}{\Delta} \int_{\alpha}^{\beta} G\left(\frac{\xi - \eta}{\Delta}, \xi\right) \phi(\eta)\, d\eta, \tag{1}$$

where G is a filter function, which, in general, can have different shapes in various regions of the domain. This definition is more general then the one commonly used in the LES literature and, as will be shown later, is crucial for elimination of boundary terms in the commutation error. The introduction of filters of different shapes in different parts of the domain is necessitated by considering inhomogeneous (nonperiodic) fields. If we assume that the function $\phi(\xi)$ is homogeneous (periodic) in $[\alpha, \beta]$, then a periodic filter can have the same shape throughout the domain.

The filtering operation in physical space can be written as

$$\bar{\psi}(x) = \frac{1}{\Delta} \int_{a}^{b} G\left(\frac{f(x) - f(y)}{\Delta}, f(x)\right) \psi(y)\, f'(y)\, dy. \tag{2}$$

Note that definitions (1) and (2) are equivalent. However, for practical purposes, the filtering operation (1) in the mapped space is much easier than (2), and we will use the former throughout unless stated otherwise.

Commutation Error in One Spatial Dimension

Let us consider first the commutation error of filtering and derivative operations in one spatial dimension. We define an operator that measures commutation error by

$$\left[\frac{d\psi}{dx}\right] \equiv \overline{\frac{d\psi}{dx}} - \frac{d\bar{\psi}}{dx}. \tag{3}$$

If we differentiate $\bar{\psi}(x)$ with respect to x and use the chain rule, we obtain

$$\frac{d\bar{\psi}}{dx}(x) = \frac{d\bar{\phi}}{d\xi}(\xi)\, f'(x), \tag{4}$$

where the filtering operation (1) is used for $\bar{\phi}$. Introducing the change of variables $\eta = \xi - \Delta\zeta$, Eq. (1) can be rewritten as

$$\bar{\phi}(\xi) = \int_{\frac{\xi-\beta}{\Delta}}^{\frac{\xi-\alpha}{\Delta}} G(\zeta, \xi)\phi(\xi - \Delta\zeta)\, d\zeta. \tag{5}$$

Performing the formal Taylor series expansion of $\phi(\xi - \Delta\zeta)$ in powers of Δ we obtain

$$\phi(\xi - \Delta\zeta) = \sum_{k=0}^{+\infty} \frac{(-1)^k}{k!}\Delta^k \zeta^k D_\xi^k \phi(\xi), \tag{6}$$

where $D_\xi^k \equiv d^k/d\xi^k$ is the derivative operator. In general, the radius of convergence of (6) is finite and determined by properties of $\phi(\xi)$. Nevertheless, if we assume that the spectrum of $\phi(\xi)$ does not include wavenumbers higher than some finite cutoff wavenumber $k_{\max}$, then as is shown in Appendix A, the series (6) is uniformly convergent everywhere in the domain $\xi \in [\alpha, \beta]$. This assumption is justified by the fact that in actual numerical simulations the wavenumber range is limited by the support of computational mesh. Therefore, without loss of generality, we consider the radius of convergence of (6) to be infinite. Under this assumption, $\phi(\xi - \Delta\zeta)$ and its Taylor series are interchangeable. Consequently, substituting (6) into (5), and changing the order of summation and integration we obtain

$$\bar{\phi}(\xi) = \sum_{k=0}^{+\infty} \frac{(-1)^k}{k!}\Delta^k \left(\int_{\frac{\xi-\beta}{\Delta}}^{\frac{\xi-\alpha}{\Delta}} \zeta^k G(\zeta, \xi)\, d\zeta \right) D_\xi^k \phi(\xi). \tag{7}$$

Let $M^k(\xi)$ be the kth filter moment defined by

$$M^k(\xi) = \int_{\frac{\xi-\beta}{\Delta}}^{\frac{\xi-\alpha}{\Delta}} \zeta^k G(\zeta, \xi)\, d\zeta. \tag{8}$$

Note that ζ is a nondimensional variable and thus all filter moments $M^k(\xi)$ $(k \geq 0)$ are nondimensional quantities. With this definition Eq. (7) can be rewritten as

$$\bar{\phi}(\xi) = \sum_{k=0}^{+\infty} \frac{(-1)^k}{k!} \Delta^k M^k(\xi) D_\xi^k \phi(\xi). \tag{9}$$

This series, as shown in Appendix A, may have either infinite or finite radius of convergence depending on the filter moments. We will later show that for the discrete filters the radius of convergence of series (9) is infinity.

Substituting (9) into (4) gives

$$\frac{d\bar{\psi}}{dx}(x) = f'(x) \sum_{k=0}^{+\infty} \frac{(-1)^k}{k!} \Delta^k \left(\frac{dM^k(\xi)}{d\xi} D_\xi^k + M^k(\xi) D_\xi^{k+1} \right) \phi(\xi). \tag{10}$$

Applying the filtering operation (2) to $\frac{d\psi}{dx}$ and using the fact that

$$\frac{d\psi}{dx}(x) = \frac{d\phi}{d\xi}(\xi) f'(x) \tag{11}$$

we obtain that

$$\overline{\frac{d\psi}{dx}}(x) = \frac{1}{\Delta} \int_\alpha^\beta G\left(\frac{\xi - \eta}{\Delta}, \xi \right) \frac{d\phi}{d\eta}(\eta) f'(F(\eta))\, d\eta. \tag{12}$$

Introducing the change of variables $\eta = \xi - \Delta\zeta$ and performing the formal Taylor series expansion in powers of Δ we obtain

$$f'(F(\eta)) = \sum_{l=1}^{+\infty} \frac{1}{(l-1)!} \left(\sum_{k=1}^{+\infty} \frac{(-1)^k}{k!} \Delta^k \zeta^k D_\xi^k F(\xi) \right)^{l-1} D_x^l f(x), \tag{13}$$

$$\frac{d\phi}{d\eta}(\eta) = \sum_{k=0}^{+\infty} \frac{(-1)^k}{k!} \Delta^k \zeta^k D_\xi^{k+1} \phi(\xi). \tag{14}$$

In numerical applications, the mapping function is evaluated on a discrete mesh. Thus, the assumption that the spectrum of mapping function does not contain high frequencies is also valid. Consequently, without loss of generality the radii of convergence of series (9), (10), (13), (14) can be considered to be infinity, and thus the original functions and their Taylor series are interchangeable. Substituting (13) and (14) into (12), using a procedure analogous to (7) and (9), and subtracting (10) from the resulting equation we obtain

$$\left[\frac{d\psi}{dx} \right] = \sum_{k=1}^{+\infty} A_k M^k(\xi) \Delta^k + \sum_{k=0}^{+\infty} B_k \frac{dM^k}{d\xi}(\xi) \Delta^k, \tag{15}$$

where A_k $(k \geq 1)$ and B_k $(k \geq 0)$ are, in general, nonzero coefficients. Thus, as can easily be seen, the commutation error is determined by filter moments $M^k(\xi)$ and mapping function $F(\xi)$.

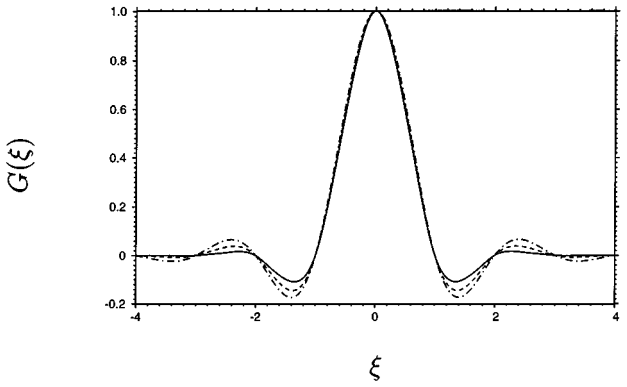

FIG. 1. Filter $G(\xi)$ (correlation function of Daubechies scaling function) with 5 (—), 9 (– – –), and 17 (– · –) vanishing moments.

In this paper we consider a general class of filters which satisfy the properties

$$M^0(\xi) = 1 \qquad \text{for } \xi \in [\alpha, \beta]; \tag{16a}$$

$$M^k(\xi) = 0 \qquad \text{for } k = 1, \ldots, n-1 \text{ and } \xi \in [\alpha, \beta]; \tag{16b}$$

$$M^k(\xi) \qquad \text{exist for } k \geq n. \tag{16c}$$

There are many examples of filters which satisfy these properties when the function $\phi(\xi)$ is defined in the domain $(-\infty, +\infty)$. One is the exponentially decaying filter defined in [2]. Another example is the correlation function of the Daubechies scaling function used in multiresolution analysis for constructing orthonormal wavelet bases. The correlation function is characterized by local support and has $2N-1$ vanishing moments, where N is the order of the Daubechies scaling function. For details we refer to [8,9]. Examples of such filters with 5, 9, and 17 vanishing moments are shown in Fig. 1. The corresponding Fourier transforms, $\hat{G}(k) = \int_{-\infty}^{+\infty} G(\xi) \exp(-ik\xi)\, d\xi$, are presented in Fig. 2. We also note that the definition (16) does not require that the filter kernel be symmetric. This allows us to use a wider class of filters than in [1,2]. We do not present continuous filters which satisfy definitions (16a)–(16c), since, as will be shown later, for practical purposes, we

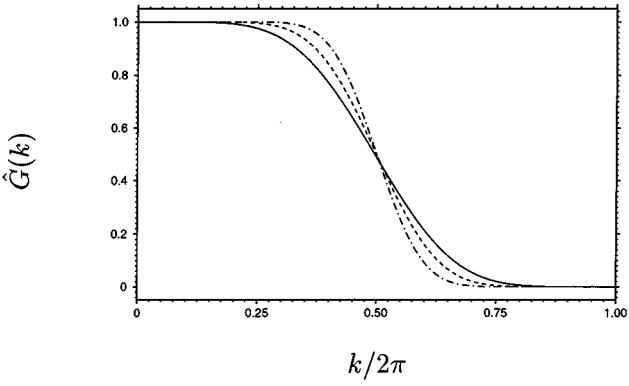

FIG. 2. Fourier transform $\hat{G}(k)$ of the filters $G(\xi)$ shown in Fig. 1.

need discrete filters. For now we only assume that such filters exist and that they can be constructed.

Using properties (16a) and (16b) it follows that

$$\frac{dM^k}{d\xi}(\xi) = 0 \qquad \text{for } k = 0, \ldots, n-1. \tag{17}$$

Consequently, the commutation error (15) is

$$\left[\frac{d\psi}{dx}\right] = \mathrm{O}(\Delta^n). \tag{18}$$

It is easy to show that in the homogeneous (periodic) case, when the shape of the filter does not depend on the location, and the mapping from the physical to the computational domain is linear, A_k is exactly zero for any k and the filter moments are not functions of the location. This results in zero commutation error.

Generalization to Multiple Dimensions

The nonuniform filtering operation in one spatial dimension can be extended easily to three spatial dimensions. Let us consider a three-dimensional field $\psi(\mathbf{x})$ ($\mathbf{x} = (x_1, x_2, x_3)^{\mathrm{T}}$) defined in three-dimensional domain $\mathbf{D}$. Let us consider a nonlinear map of the physical space domain $\mathbf{D}$ into a rectangular domain $\Omega = [\alpha_1, \beta_1] \times [\alpha_2, \beta_2] \times [\alpha_3, \beta_3]$ given by $\boldsymbol{\xi} = \mathbf{f}(\mathbf{x})$, where $\boldsymbol{\xi} = (\xi_1, \xi_2, \xi_3)^{\mathrm{T}}$. As in the one-dimensional case this transformation can be associated with the mapping of a spatially nonuniform computational grid to a uniform grid with spacings Δ_1, Δ_2, Δ_3 in the corresponding directions. Let $\mathbf{x} = \mathbf{F}(\boldsymbol{\xi})$ be the inverse mapping.

The three-dimensional filtering operation is defined the same way as in one spatial dimension. Given an arbitrary function $\psi(\mathbf{x})$ we obtain the new function $\phi(\boldsymbol{\xi}) = \psi(\mathbf{F}(\boldsymbol{\xi}))$ defined in the domain Ω. The function $\phi(\boldsymbol{\xi})$ is then filtered using a sequence of three one-dimensional filters. Thus the filtering operation in three spatial dimensions is defined by

$$\bar{\phi}(\boldsymbol{\xi}) = \oint_{\Omega} \prod_{i=1}^{3} \frac{1}{\Delta_i} G\left(\frac{\xi_i - \eta_i}{\Delta_i}, \xi_i\right) \phi(\boldsymbol{\eta})\, d^3\boldsymbol{\eta}, \tag{19}$$

where $\oint_{\Omega}$ is the volume integral over domain Ω. The filtering operation in physical space can be written as

$$\bar{\psi}(\mathbf{x}) = \oint_{\mathbf{D}} \prod_{i=1}^{3} \frac{1}{\Delta_i} G\left(\frac{f_i(\mathbf{x}) - f_i(\mathbf{y})}{\Delta_i},\ f_i(\mathbf{x})\right) \psi(\mathbf{y}) J(\mathbf{y})\, d^3\mathbf{y}, \tag{20}$$

where $J(\mathbf{y})$ is the Jacobian of the transformation $\boldsymbol{\xi} \to \mathbf{x}$. Note that the filtering operations (19) and (20) are equivalent, but (19) is more convenient than (20) for both the analysis of the commutation error and practical purposes. We will use (19) in what follows unless stated otherwise.

If one performs the same type of analysis as in the one-dimensional case, it is easy to show (see Appendix B) that the commutation error in three spatial dimensions is given by

$$\left[\frac{\partial\psi}{\partial x_k}\right] = \mathrm{O}\left(\Delta_1^n, \Delta_2^n, \Delta_3^n\right). \tag{21}$$

Thus, the commutation error of differentiation and filtering operation is no more than the error introduced by an nth-order finite difference scheme, provided that the filter has $n-1$ zero moments.

Boundary Conditions for Filterd Field

It is well known that the boundary conditions for the filtered field are not necessarily the same as those for the nonfiltered field. Nevertheless the boundary conditions for the nonfiltered field, which we will call physical boundary conditions, are still commonly used in large eddy simulations. In this section we will justify the use of the unfiltered field boundary conditions for LES, at least when local structures are of the order of filter width or larger and the appropriate filter is used.

Equations (B2) and (B4) in Appendix B are valid in every point of the domain. Thus, applying these equations to any point $\mathbf{x}$ at the boundary of the domain and using the fact that the first $n-1$ moments are zero together with (17) we obtain

$$\bar{\psi}(\mathbf{x}) = \psi(\mathbf{x}) + \mathrm{O}\left(\Delta_1^n, \Delta_2^n, \Delta_3^n\right), \tag{22a}$$

$$\frac{\partial \bar{\psi}}{\partial x_k}(\mathbf{x}) = \frac{\partial \psi}{\partial x_k}(\mathbf{x}) + \mathrm{O}\left(\Delta_1^n, \Delta_2^n, \Delta_3^n\right). \tag{22b}$$

The difference between the boundary conditions for the filtered and unfiltered fields is of the order n. Thus the physical boundary conditions can be used for the filtered field. Note that, if desired, the number of vanishing moments for the filter close to the boundary can be larger than that in the middle of the domain. Thus the boundary conditions for the filtered field can approach the physical boundary conditions up to the desired order of accuracy, provided that all local structures are appropriately resolved.

III. CONSISTENT DISCRETE FILTERING IN COMPLEX GEOMETRY

In large eddy simulation of turbulent flows, the solution is available only on a set of discrete grid points, and thus discrete filters are required in various operations. The machinery developed in Section II can be adapted to discrete filtering. In this section we will limit ourselves to consideration of discrete one-dimensional filtering, since three-dimensional filtering can be considered as an application of a sequence of three one-dimensional filters. Also, since the filtering operation is performed in the mapped space, we will consider only the case of uniformly sampled data.

Construction of Discrete Filters

Let us consider a one-dimensional field $\phi(\xi)$ defined in the domain $[\alpha, \beta]$. $\{\phi_j\}$ corresponds to values of $\phi(\xi_j)$ at locations $\xi_j = \alpha + \Delta j$ $(j = 0, \ldots, N)$, where Δ is the sampling interval. A one-dimensional filter is defined by

$$\frac{1}{\Delta} G\left(\frac{\xi_j - \eta}{\Delta}, \xi_j\right) = \sum_{l=-K_j}^{L_j} \mathrm{w}_l^j \delta(\eta - \xi_{j+l}), \tag{23}$$

where $\delta(\xi)$ is a δ-function with the property

$$\int_\alpha^\beta \phi(\eta)\delta(\eta-\xi)\,d\eta = \phi(\xi) \tag{24}$$

and w_l^j are weight factors. We consider the general class of asymmetric filters for which $K_j \neq L_j$. One of the important aspects of discrete filters is that all filter moments exist and condition (A10) holds, which means that the radii of convergence of Taylor series (9) and other related series are infinite. Substitution of (23) into (1) gives the following definition for a discrete filter:

$$\bar{\phi}_j = \sum_{l=-K_j}^{L_j} \mathrm{w}_l^j \phi_{j+l}. \tag{25}$$

Property (23) allows us to apply results of Section II to discrete filters.

In light of the filter definition (16), the weight factors should satisfy the properties

$$\sum_{l=-K_j}^{L_j} \mathrm{w}_l^j = 1, \tag{26a}$$

$$\sum_{l=-K_j}^{L_j} l^m \mathrm{w}_l^j = 0, \qquad m = 1,\ldots,n-1. \tag{26b}$$

Equations (26) give us n constraints on w_l^j and are solvable if and only if $L_j + K_j + 1 \geq n$. If $L_j + K_j + 1 > n$ then additional constraints can be applied.

Conditions (26) give the minimum number of degrees of freedoms for a discrete filter in order for the derivative and filtering operations to commute to order n. This condition gives the minimum filter support, which can be increased by adding additional constraints. The additional linear or nonlinear constraints can be altered depending on the desired shape of the Fourier transform $\hat{G}(k)$ associated with the filter (23) given by

$$\hat{G}(k) = \sum_{l=-K_j}^{L_j} \mathrm{w}_l^j e^{-i\Delta k l}. \tag{27}$$

A desirable constraint on a Filter is that its Fourier transform be zero at the cutoff frequency, i.e., $\hat{G}(\pi/\Delta) = 0$. The mathematical equivalent of this requirement is given by

$$\sum_{l=-K_j}^{L_j} (-1)^l \mathrm{w}_l^j = 0. \tag{28}$$

Conditions (26) and (28) represent the minimum number of constraints which should be imposed on the filter. Examples of weights for minimally constrained discrete filters are given in Table I, and associated Fourier transforms for some of these filters are presented in Figs. 3–5. Examples of the Fourier transforms of minimally constrained symmetric filters with one, three, and five vanishing moments are presented in Fig. 3. These filters correspond respectively to cases 1, 6, and 10 presented in Table I. We see that with the increase in the number of vanishing moments, filter becomes a better approximation to the sharp cutoff

TABLE I

Values of the Weight Factors and the Number of Vanishing Moments for Different Minimally Constrained Discrete Filters

Case	Number of vanishing moments	w_{-3}	w_{-2}	w_{-1}	w_0	w_1	w_2	w_3	w_4	w_5
1	1			$\frac{1}{4}$	$\frac{1}{2}$	$\frac{1}{4}$				
2	2				$\frac{7}{8}$	$\frac{3}{8}$	$-\frac{3}{8}$	$\frac{1}{8}$		
3	2			$\frac{1}{8}$	$\frac{5}{8}$	$\frac{3}{8}$	$-\frac{1}{8}$			
4	3				$\frac{15}{16}$	$\frac{1}{4}$	$-\frac{3}{8}$	$\frac{1}{4}$	$-\frac{1}{16}$	
5	3			$\frac{1}{16}$	$\frac{3}{4}$	$\frac{3}{8}$	$-\frac{1}{4}$	$\frac{1}{16}$		
6	3		$-\frac{1}{16}$	$\frac{1}{4}$	$\frac{5}{8}$	$\frac{1}{4}$	$-\frac{1}{16}$			
7	4				$\frac{31}{32}$	$\frac{5}{32}$	$-\frac{5}{16}$	$\frac{5}{16}$	$-\frac{5}{32}$	$\frac{1}{32}$
8	4			$\frac{1}{32}$	$\frac{27}{32}$	$\frac{5}{16}$	$-\frac{5}{16}$	$\frac{5}{32}$	$-\frac{1}{32}$	
9	4		$-\frac{1}{32}$	$\frac{5}{32}$	$\frac{11}{16}$	$\frac{5}{16}$	$-\frac{5}{32}$	$\frac{1}{32}$		
10	5	$\frac{1}{64}$	$-\frac{3}{32}$	$\frac{15}{64}$	$\frac{11}{16}$	$\frac{15}{64}$	$-\frac{3}{32}$	$\frac{1}{64}$		

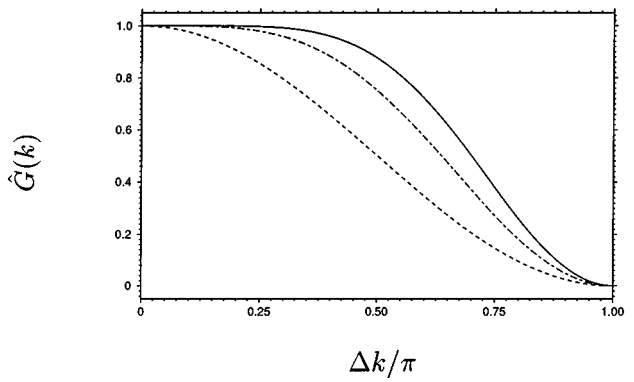

FIG. 3. Fourier transform $\hat{G}(k)$ of the symmetric minimally constrained discrete filters with one (– – –), three (– · –), and five (—) vanishing moments corresponding respectively to cases 1, 6, and 10 given in Table I.

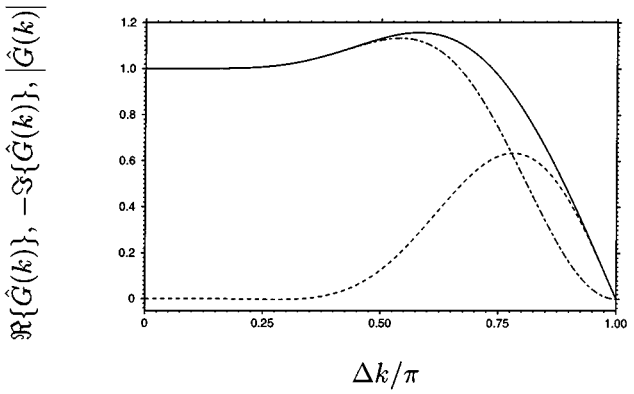

FIG. 4. Real $\Re\{\hat{G}(k)\}$ (– · –), imaginary $\Im\{\hat{G}(k)\}$ (– – –), and absolute value $|\hat{G}(k)|$ (—) of Fourier tranform $\hat{G}(k)$ of the asymmetric discrete filter with four vanishing moments corresponding to case 8 given in Table I.

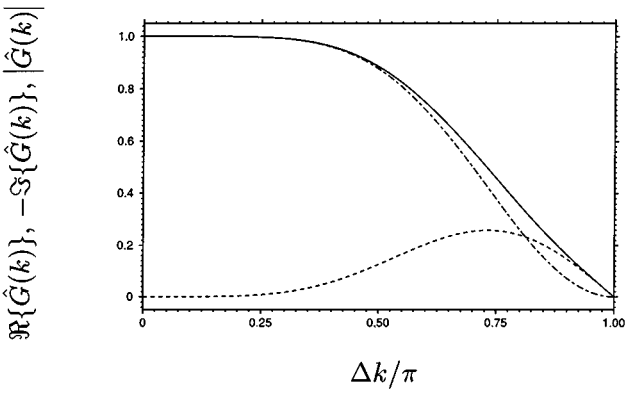

FIG. 5. Real $\Re\{\hat{G}(k)\}$ $(-\cdot-)$, imaginary $\Im\{\hat{G}(k)\}$ $(---)$, and absolute value $|\hat{G}(k)|$ (—) of Fourier transform $\hat{G}(k)$ of the asymmetric discrete filter with four vanishing moments corresponding to case 9 given in Table I.

filter, which is more appealing from the physical point of view. It also can be observed that filters shown in Fig. 3 have different effective cutoff frequencies. Thus in order to control the effective cutoff frequency, additional constraints should be introduced. The Fourier transform of asymmetric filters with four vanishing moments corresponding to cases 8 and 9 presented in Table I are shown in Figs. 4 and 5, correspondingly. Note that the asymmetric filters introduce phase shifts due to their nonzero imaginary parts. The imaginary part should be minimized by introducing additional constraints. Also notice the overshoot in the real part and absolute value of the filter shown in Fig. 4. In general, an overshoot is not desirable since it may lead to nonphysical growth of energy. Additional constraints are necessary in order to reduce or remove overshoot.

In the interior of the domain, in order to eliminate the phase shift, the filter should be symmetric; i.e., the following relation should be satisfied:

$$\mathrm{w}_l^j = \mathrm{w}_{-l}^j, \qquad l = 1, \ldots, L, \tag{29a}$$

$$L_j = K_j = L. \tag{29b}$$

In this case the filter only adjusts the amplitude of a given wavenumber component of the solution and leaves its phase unchanged. Near the boundaries, however, it may be necessary to make the filter asymmetric. In this case a phase shift is introduced and one is interested in minimizing this effect.

Examples shown in Figs. 3–5 demonstrate the necessity of the introduction of additional constraints which ensure that the resulting filter has all the desired properties. One way to constrain the filter is to specify either its value

$$\hat{G}(k) = \sum_{l=-K_j}^{L_j} \mathrm{w}_l^j \, e^{-i\,\Delta k l} \tag{30a}$$

or the value of its derivative

$$\hat{G}^{(m)}(k) = \sum_{l=-K_j}^{L_j} (-i\,\Delta k l)^m \mathrm{w}_l^j e^{-i\,\Delta k l} \tag{30b}$$

for a given frequency k. Examples of weights for filters with three vanishing moments and different linear constraints are given in Table II, and associated Fourier transforms

TABLE II
Values of the Weight Factors and the Number of Vanishing Moments for Different Linearly Constrained Discrete Filters

Case	Number of vanishing moments	Additional constraints	w_0	$w_{\pm1}$	$w_{\pm2}$	$w_{\pm3}$	$w_{\pm4}$	$w_{\pm5}$
1	3	$\hat{G}(\frac{\pi}{3\Delta}) = 1/2$ $\hat{G}^{(m)}(\frac{\pi}{\Delta}) = 0,\ m = 0, \ldots, 5$	$\frac{373}{1152}$	$\frac{911}{3456}$	$\frac{203}{1728}$	$-\frac{11}{2304}$	$-\frac{203}{6912}$	$-\frac{61}{6912}$
2	3	$\hat{G}(\frac{\pi}{2\Delta}) = 1/2$ $\hat{G}^{(m)}(\frac{\pi}{\Delta}) = 0,\ m = 0, \ldots, 1$	$\frac{1}{2}$	$\frac{9}{32}$	0	$-\frac{1}{32}$		
3	3	$\hat{G}(\frac{2\pi}{3\Delta}) = 1/2$ $\hat{G}^{(m)}(\frac{\pi}{\Delta}) = 0,\ m = 0, \ldots, 1$	$\frac{47}{72}$	$\frac{35}{144}$	$-\frac{11}{144}$	$\frac{1}{144}$		

for these filters are presented in Fig. 6. These filters are constrained in such a way that the effective filter widths are 3Δ, 2Δ, and $3/2\Delta$ (corresponding to characteristic wavenumbers $\Delta k/\pi = 1/3, 1/2, 2/3$). We observed that for the filters with relatively small characteristic wavenumbers, the number of zero derivatives at $k = \pi/\Delta$ should be considerably larger than for filters with characteristic wavenumbers close to π/Δ. If we chose this number small enough, then the value of the Fourier transform of the filter for frequencies larger then characteristic wavenumber may reach a large amplitude. Thus setting the large number of derivatives at $k = \pi/\Delta$ forces the filter to have the desired shape.

Alternative Construction of Filters with Desired Properties

Linear constraints of the form (30) are often enough to obtain the desired filter. However, there are situations, especially for asymmetric filters, where it is difficult to choose a limited number of constraints such that the filter is close to the desired shape. It is much more desirable to specify the target filter function $\hat{G}_t(k)$ and to construct a filter which will be close to it. One way of doing so is to find the set of filter weights which satisfy all linear

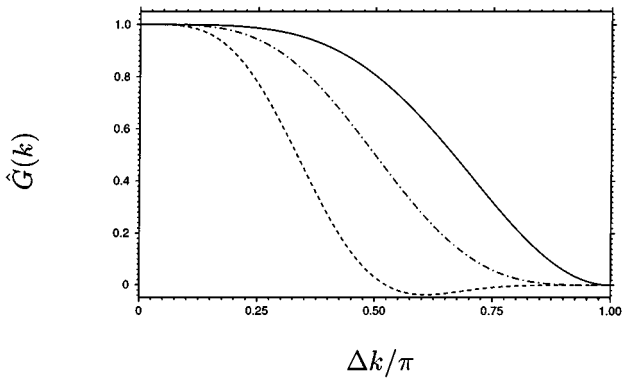

FIG. 6. Fourier transform $\hat{G}(k)$ of the symmetric discrete filters with different additional linear constraints corresponding to cases 1 (– – –), 2 (– · –), and 3 (—) given in Table II.

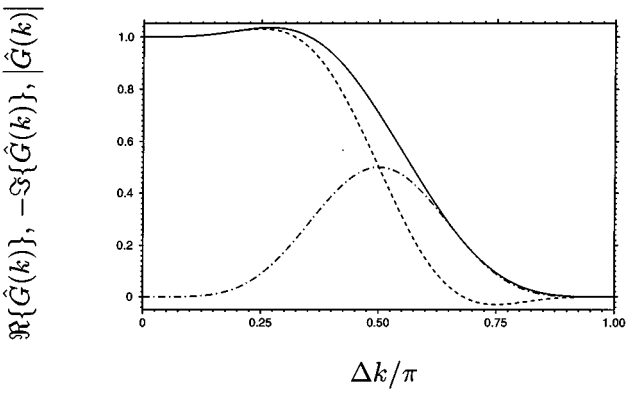

FIG. 7. Real $\Re\{\hat{G}(k)\}$ $(-\cdot-)$, imaginary $\Im\{\hat{G}(k)\}$ $(--)$, and absolute value $|\hat{G}(k)|$ (—) of Fourier transform $\hat{G}(k)$ of the asymmetric discrete filter with three vanishing moments obtained using only linear constraints.

constraints and minimize the functional

$$\int_0^{\pi/\Delta} (\Re\{\hat{G}(k) - \hat{G}_t(k)\})^2\, dk + \int_0^{\pi/\Delta} (\Im\{\hat{G}(k) - \hat{G}_t(k)\})^2\, dk, \tag{31}$$

where $\Re\{z\}$ and $\Im\{z\}$ denote correspondingly real and imaginary parts of a complex number z. Note that integral ranges as well as relative weights for real and imaginary contributions to the functional can be arbitrarily set depending on the filter function $\hat{G}_t(k)$. The mathematical details of the minimization are given in Appendix C. Figure 7 shows an example of an asymmetric filter with an eight-point stencil ($K=2$ and $L=5$). The real part of the filter is constrained to be $1/2$ at $\Delta k/\pi = 1/2$. The filter value and its first two derivatives are constrained to be zero at $k=\pi/\Delta$. In order to improve the filter's characteristics the minimization was performed, where requirements for two derivatives at $k=\pi/\Delta$ were relaxed and quadratic minimization as described in Appendix C was used instead. The resulting filter is shown in Fig. 8. Comparing both filters we can see that the filter presented in Fig.8 has better characteristics. We found that, in general, the minimization procedure gives better filters than the ones obtained using only linear constraints.

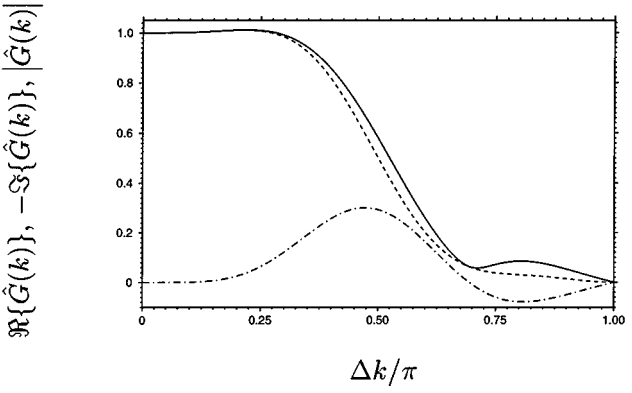

FIG. 8. Real $\Re\{\hat{G}(k)\}$ $(-\cdot-)$, imaginary $\Im\{\hat{G}(k)\}$ $(--)$, and absolute value $|\hat{G}(k)|$ (—) of Fourier transform $\hat{G}(k)$ of the asymmetric discrete filter with three vanishing moments obtained using quadratic minimization.

Pade Filters

Discrete filters presented in this section can be considered as one example of an entire class of discrete filters with vanishing moments. Other discrete filters can be utilized as well. For example, one useful extension of the present algorithm is to use Pade-type filters which are given by

$$\sum_{m=-M_j}^{N_j} \mathrm{v}_m^j \bar{\phi}_{j+m} = \sum_{l=-K_j}^{L_j} \mathrm{w}_l^j \phi_{j+l} \tag{32}$$

and require the solution of linear systems of equations. The Fourier transform $\hat{G}(k)$ associated with Pade-type filters is given by

$$\hat{G}(k) = \frac{\sum_{l=-K_j}^{L_j} \mathrm{w}_l^j \, e^{-i\Delta kl}}{\sum_{m=-M_j}^{N_j} \mathrm{v}_m^j \, e^{-i\Delta km}}. \tag{33}$$

In the case of Pade filters, conditions (26) can be rewritten as

$$\sum_{l=-K_j}^{L_j} \mathrm{w}_l^j = 1, \tag{34a}$$

$$\sum_{m=-M_j}^{N_j} \mathrm{v}_m^j = 1, \tag{34b}$$

$$\sum_{m=-M_j}^{N_j} m^i \mathrm{v}_m^j = \sum_{l=-K_j}^{L_j} l^i \mathrm{w}_l^j, \qquad i = 1, \ldots, n-1. \tag{34c}$$

It is straightforward to constrain Pade filters to a specific value at specific frequency. Nevertheless, linear constraining of filter derivatives $\hat{G}^{(m)}(k)$ at a certain frequency requires additional specification of filter value as well as all previous derivatives. For more details of Pade filters we refer to [10].

The use of Pade-type filters gives more flexibility in constructing filters which are closer to spectral cutoff filters. Examples of weights for symmetric ($M_j = N_j$ and $K_j = L_j$) Pade filters with five vanishing moments and different linear constraints are given in Table III, and associated Fourier transforms are presented in Fig. 9. Comparing Figs. 6 and 9 it can be seen that Pade filters are considerably better approximations of sharp cutoff filters.

Commutation Error of Discrete Filtering and Differentiation

In Section II we demonstrated that the commutation error of continuous filtering and differentiation operators is determined by the number of vanishing moments of the continuous filter. As was mentioned earlier in this section, the same conclusion is valid for discrete filters. In order to validate that discrete filtering and differentiation commute up to the same order, we perform a numerical test, in which we differentiate numerically the Chebyshev polynomial of the 16th order and determine the commutation error of discrete filtering and differentiation operators. Since the derivative of the Chebyshev polynomial can

TABLE III
Values of the Weight Factors for Different Linearly Constrained Symmetric Pade Filters with Five Vanishing Moments

Case	Additional constraints	v_0	$v_{\pm1}$	$v_{\pm2}$	$v_{\pm3}$	w_0	$w_{\pm1}$	$w_{\pm2}$	$w_{\pm3}$	$w_{\pm4}$	$w_{\pm5}$
1	$\hat{G}(\frac{\pi}{3\Delta})=1/2$ $\hat{G}^{(m)}(\frac{\pi}{\Delta})=0,\ m=0,\ldots,9$	$\frac{543}{128}$	$-\frac{1405}{512}$	$\frac{313}{256}$	$-\frac{51}{512}$	$\frac{63}{256}$	$\frac{105}{512}$	$\frac{15}{128}$	$\frac{45}{1024}$	$\frac{5}{512}$	$\frac{1}{1024}$
2	$\hat{G}(\frac{\pi}{2\Delta})=1/2$ $\hat{G}^{(m)}(\frac{\pi}{\Delta})=0,\ m=0,\ldots,7$	$\frac{7}{12}$	0	$\frac{5}{24}$		$\frac{7}{24}$	$\frac{175}{768}$	$\frac{5}{48}$	$\frac{35}{1536}$	0	$-\frac{1}{1536}$
3	$\hat{G}(\frac{2\pi}{3\Delta})=1/2$ $\hat{G}^{(m)}(\frac{\pi}{\Delta})=0,\ m=0,\ldots,3$	$\frac{49}{120}$	$\frac{13}{60}$	$\frac{19}{240}$		$\frac{11}{30}$	$\frac{119}{480}$	$\frac{1}{15}$	$\frac{1}{480}$		

be calculated exactly, we can calculate the truncation error of the numerical differentiation as well. We choose the nonuniform computational mesh to be given by

$$x_j = -\frac{\tanh(\gamma(1-2j/N_g))}{\tanh(\gamma)}, \tag{35}$$

where N_g is the total number of grid points and γ is the stretching parameter. The choice for the hyperbolic grid stretching is motivated by its frequent use in both DNS and LES simulations of wall-bounded flows. For the hyperbolic tangent grid, the ratio of largest to smallest grid size is a function of stretching parameter γ and is given by $\cosh^3\gamma/\sinh\gamma$. In this test we choose $\gamma = 2.75$, which makes this ratio approximately 62. The differentiation operator is chosen to be fourth-order accurate on the nonuniform grid. Figure 10 shows the truncation error of finite difference scheme and commutation errors as a function of the total number of gird points for filters with different number of zero moments. The results presented in Fig. 10 confirm that the discrete filtering and differentiation operators commute up to the nth order, provided that the discrete filter has $n-1$ vanishing moments.

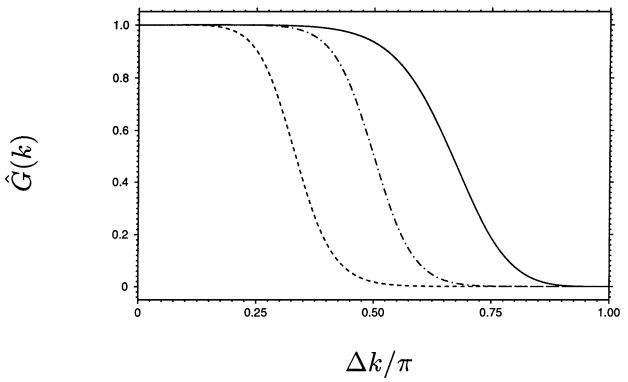

FIG. 9. Fourier transformation $\hat{G}(k)$ of the symmetric Pade filters with different additional linear constraints corresponding to cases 1 (– – –), 2 (–·–), and 3 (—) given in Table III.

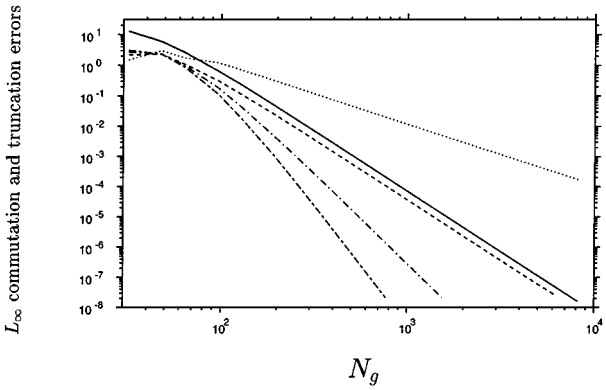

FIG. 10. Truncation error (—) of the differentiation operator and commutation error for discrete filtering and differentiation operations for the filters with one (· · ·), three (– – –), five (– · –), and seven (– – –) vanishing moments.

IV. EQUATIONS FOR LARGE EDDY SIMULATION AND DISCRETE FILTERING

If we apply the continuous filtering operation (20) with nonuniform filter width to the Navier–Stokes equations and ignore terms of order $O(\Delta_i^n)$, associated with the residual commutation error, we obtain the filtered equations of motion. For an incompressible flow the nondimensional equations take the form

$$\frac{\partial \bar{u}_i}{\partial x_i} = 0, \tag{36}$$

$$\frac{\partial \bar{u}_i}{\partial t} + \frac{\partial \overline{u_i u_j}}{\partial x_j} = -\frac{\partial \bar{p}}{\partial x_i} + \frac{1}{\mathrm{Re}} \frac{\partial^2 \bar{u}_i}{\partial x_j \partial x_j}. \tag{37}$$

Equation (37) can be rewritten in the form

$$\frac{\partial \bar{u}_i}{\partial t} + \frac{\partial \overline{u_i u_j}}{\partial x_j} = -\frac{\partial \bar{p}}{\partial x_i} - \frac{\partial \bar{\tau}_{ij}}{\partial x_j} + \frac{1}{\mathrm{Re}} \frac{\partial^2 \bar{u}_i}{\partial x_j \partial x_j}, \tag{38}$$

where the effect of small scales appears through the SGS stress term given by

$$\bar{\tau}_{ij} = \overline{u_i u_j} - \overline{u_i} \overline{u_j}, \tag{39}$$

which should be modeled. Note that in contrast with standard LES formulation, the nonlinear terms such as $\bar{u}_i \bar{u}_j$ and τ_{ij} are treated with a secondary filtering operation to eliminate the generation of frequencies higher than the characteristic wavenumber for the chosen filter. This is how the filter operator enters the solution procedure. The resulting (explicitly) filtered Navier–Stokes equations (36), (38), (39) govern the evolution of large scales of motion. As was demonstrated in the previous sections, the boundary conditions for filtered velocity components can be taken to be the physical boundary conditions.

A possible drawback of this new formulation is that Eq. (38) is not Galilean invariant provided that modeled subgrid-scale stresses (39) are Galilean invariant and nonsharp cutoff filter is utilized. Non-Galilean invariance follows from the appearance of the term

$c_j \partial(\overline{\overline{u}}_i - \overline{u}_i)/\partial x_j$, where c_j is the uniform translation velocity. The error is seen to be proportional to the difference between the singly and doubly filtered velocity. This difference will be zero for a sharp cutoff filter, but will not vanish in the general case. The spectral content of the error is proportional to $\hat{G}(\mathbf{k})(1-\hat{G}(\mathbf{k}))$, where $\hat{G}(\mathbf{k})$ is the filter transfer function and $\mathbf{k}$ is the wave vector. This fact implies that error is only generated in the wavenumber band where $\hat{G}(\mathbf{k})$ differs significantly from 0 or 1. Thus it is possible to minimize the error by constructing the explicit filter to be as close as possible to a sharp cutoff.

The subgrid-scale stress (39) can be modeled using the dynamic procedure as in [5,6]. The dynamic procedure can utilize different models. We will illustrate the dynamic procedure using the Smagorinsky model given by

$$\overline{\tau}_{ij} - \frac{1}{3}\delta_{ij}\overline{\tau}_{kk} = -2\Delta^2\,\overline{C|S|S_{ij}}, \tag{40}$$

where δ_{ij} is the Kronecker delta, $\overline{S}_{ij} = (\partial\overline{u}_i/\partial x_j + \partial\overline{u}_j/\partial x_i)/2$, $|\overline{S}| = (2\overline{S}_{ij}\overline{S}_{ij})^{1/2}$, C is the Smagorinsky coefficient, and Δ is the effective filter width. Once again the nonlinear terms are filtered to ensure that they have the same frequency content as other terms of the equations.

If we apply a coarser spatial filter, called the "test" filter, to the filtered Navier–Stokes equation (38) we obtain

$$\frac{\partial\hat{\overline{u}}_i}{\partial t} + \frac{\partial\widehat{\hat{\overline{u}}_i\hat{\overline{u}}_j}}{\partial x_j} = \frac{\partial\hat{\overline{p}}}{\partial x_i} - \frac{\partial\hat{T}_{ij}}{\partial x_j} + \frac{1}{\mathrm{Re}}\frac{\partial^2\hat{\overline{u}}_i}{\partial x_j\partial x_j}, \tag{41}$$

where subtest-scale stress

$$\hat{T}_{ij} = \widehat{\overline{u_i u_j}} - \widehat{\hat{\overline{u}}_i\hat{\overline{u}}_j} \tag{42}$$

is similarly approximated by

$$\hat{T}_{ij} - \frac{1}{3}\delta_{ij}\hat{T}_{kk} = -2\hat{\Delta}^2\,\widehat{C|\hat{S}|\hat{S}_{ij}}, \tag{43}$$

where $\hat{\Delta}$ is the effective test filter width. Note that we assumed that Smagorinsky coefficients for both subgrid- and subtest-scale stresses are the same. The resolved turbulent stresses $L_{ij} = \widehat{\overline{u_i u_j}} - \widehat{\hat{\overline{u}}_i\hat{\overline{u}}_j}$, which represent the contribution of the smallest resolved scales to the Reynolds stresses and can be computed exactly due to the explicit filtering, are related to the subgrid-scale stresses $\overline{\tau}_{ij}$ and $\hat{T}_{ij}$ by the identity

$$L_{ij} = \hat{T}_{ij} - \hat{\overline{\tau}}_{ij}. \tag{44}$$

Combining (40), (43), and (44) we obtain

$$L_{ij} - \frac{1}{3}\delta_{ij}L_{kk} = -2\hat{\Delta}^2\,\widehat{C|\hat{S}|\hat{S}_{ij}} + 2\Delta^2\,\widehat{C|\hat{S}|\hat{S}_{ij}}. \tag{45}$$

Equation (45) is solved in the least square sense in an analogous manner as in [6]. Briefly, C can be chosen to minimize the sum of the squares of the residuals $E_{ij}E_{ij}$ where the residual is given by

$$E_{ij} = L_{ij} - \frac{1}{3}\delta_{ij}L_{kk} + 2\hat{\Delta}^2\,\widehat{C|\hat{S}|\hat{S}_{ij}} - 2\Delta^2\,\widehat{C|S|S_{ij}}. \tag{46}$$

Note that C appears above only as $\Delta^2 C$ or $\hat{\Delta}^2 C$, and thus there is no need to explicitly provide the values for Δ and $\hat{\Delta}$. The only parameter which needs to be prescribed is the filter width ratio, which is given by the inverse ratio of cutoff frequencies.

In order to perform numerical simulations, Eqs. (36), (38), (39) should be discretized using a finite difference scheme of the desired order. We emphasize that the local grid spacing should be finer than the local filter width to ensure that the grid is adequate to resolve the filtered field. Consequently, if the filter width is of the same order as the computational grid, application of the filter which has $n-1$ zero moments to the Navier–Stokes equations introduces an error that is no more than the error introduced by an nth-order finite difference scheme used to discretize the LES equations. In other words, in order to perform a consistent derivation of the discrete LES equations, the filter has to have at least $n-1$ zero moments if nth-order finite differencing is used.

V. CONCLUSIONS

We have formulated general requirements for a filter having a nonuniform filter width which ensure that the differentiation and filtering operations commute to any desired order. Minimization of the commutation error is achieved by requiring that the filter has a number of vanishing moments. Application of this filter to the Navier–Stokes equations results in the standard LES equations which can be solved on a nonuniform computational grid. The commutation error can be neglected provided that the filter has $n-1$ vanishing moments, where n is the order of the numerical discretization scheme used to solve the LES equations. It was shown that the error associated with the implementation of the same boundary conditions as for Navier–Stokes equations is of the same order or smaller as the error associated with the finite difference operator. A general set of rules for constructing discrete filters in complex geometries is provided. The use of these filters ensures consistent derivation of discrete LES equations. The resulting discrete filtering operation is very simple and efficient. We have also described the general procedure for using an explicit filter in LES to obtain a solution consistent with the true filtered Navier–Stokes equations. The same filter can also be used for direct comparison between experimental and LES results.

APPENDIX A

The purpose of this appendix is to validate the use of Taylor series expansions in the analysis of the commutation error.

Let us assume that spectrum of a given one-dimensional field $\phi(\xi)$ does not contain wavenumbers higher than $k_{\max}$. Then $\phi(\xi)$ can be written in terms of the Fourier integral given by

$$\phi(\xi) = \int_{-k_{\max}}^{k_{\max}} \hat{\phi}(k)\, e^{-ik\xi}\, dk, \tag{A1}$$

where $\hat{\phi}(k)$ contains both continuous $\hat{\phi}_{\mathrm{c}}(k)$ and discrete $\hat{\phi}_{\mathrm{d}}(k_i)$ spectra given by

$$\hat{\phi}(k) = \hat{\phi}_{\mathrm{c}}(k) + \sum_{i=-L_{\mathrm{d}}}^{L_{\mathrm{d}}} \hat{\phi}_{\mathrm{d}}(k_i)\delta(k-k_i). \tag{A2}$$

The mth derivative of $\phi(\xi)$ with respect to ξ can be written as

$$\phi^{(m)}(\xi) = (-i)^m \int_{-k_{\max}}^{k_{\max}} k^m \hat{\phi}(k)\, e^{-ik\xi}\, dk, \tag{A3}$$

from which it is easy to obtain the inequality

$$\left|\phi^{(m)}(\xi)\right| \le \int_{-k_{\max}}^{k_{\max}} |k|^m |\hat{\phi}(k)|\, dk. \tag{A4}$$

Using Hölder's integral inequality we obtain

$$\left|\phi^{(m)}(\xi)\right| \le \left(\int_{-k_{\max}}^{k_{\max}} k^{2m}\, dk\right)^{1/2} \left(\int_{-k_{\max}}^{k_{\max}} |\hat{\phi}(k)|^2\, dk\right)^{1/2}. \tag{A5}$$

Writing the total energy as

$$E = \int_{-k_{\max}}^{k_{\max}} |\hat{\phi}(k)|^2\, dk \tag{A6}$$

we obtain the inequality

$$\left|\phi^{(m)}(\xi)\right| \le \left(\frac{2Ek_{\max}}{2m+1}\right)^{1/2} k_{\max}^m. \tag{A7}$$

Using (A7), the following sequence of inequalities can be obtained,

$$\begin{aligned}\left|\sum_{m=0}^{+\infty} \frac{(-1)^m}{m!} \Delta^m \zeta^m D_\xi^m \phi^{(m)}(\xi)\right| &\le \sum_{m=0}^{+\infty} \frac{\Delta^m |\zeta|^m}{m!} \left|\phi^{(m)}(\xi)\right| \\ &\le (2Ek_{\max})^{1/2} \sum_{m=0}^{+\infty} \frac{(k_{\max}\Delta|\zeta|)^m}{m!(2m+1)^{1/2}} \\ &\le (2Ek_{\max})^{1/2}\, e^{k_{\max}\Delta|\zeta|}, \end{aligned} \tag{A8}$$

which proves the absolute and thus uniform convergence of Taylor series (6).

Applying inequality (A7) to the analysis of absolute convergence of Taylor series (9) we obtain that

$$\begin{aligned}\left|\sum_{m=0}^{+\infty} \frac{(-1)^m}{m!} \Delta^m M^m(\xi)\phi^{(m)}(\xi)\right| &\le \sum_{m=0}^{+\infty} \frac{1}{m!} \Delta^m |M^m(\xi)| \left|\phi^{(m)}(\xi)\right| \\ &\le (2Ek_{\max})^{1/2} \sum_{m=0}^{+\infty} \frac{(k_{\max}\Delta)^m |M^m(\xi)|}{m!(2m+1)^{1/2}}. \end{aligned} \tag{A9}$$

Comparing two consecutive terms of the latter series, it can easily be seen that the series converges for arbitrary Δ provided that

$$\lim_{m\to\infty} \frac{|M^{m+1}(\xi)|}{|M^m(\xi)|(m+1)} = 0. \tag{A10}$$

It is easy to show that the limit always holds for filters with finite support. If the limit (A10) is finite and equal to $1/C$ then the series (9) converges under the condition that

$$k_{\max}\Delta \leq C. \tag{A11}$$

This condition holds for some filters with infinite support such as Gaussian filters.

APPENDIX B

The purpose of this appendix is to give mathematical details of the analysis of the commutation error in three spatial dimensions.

Differentiating Eq. (20), written as in (19), gives

$$\frac{\partial \bar{\psi}}{\partial x_k}(\mathbf{x}) = \sum_{j=1}^{3} \frac{\partial \bar{\phi}}{\partial \xi_j}(\boldsymbol{\xi}) \frac{\partial f_j}{\partial x_k}(\mathbf{x}). \tag{B1}$$

Introducing the change of variables $\eta_i = \xi_i - \Delta_i \zeta_i$, performing the formal Taylor series expansion in powers of Δ_i, and changing the order of summation and integration we obtain

$$\bar{\phi}(\boldsymbol{\xi}) = \left(\prod_{i=1}^{3} \sum_{k_i=0}^{+\infty} \frac{(-1)^{k_i}}{k_i!} \Delta_i^{k_i} M_i^{k_i}(\xi_i) D_{\xi_i}^{k_i} \right) \phi(\boldsymbol{\xi}), \tag{B2}$$

where

$$M_i^k(\xi_i) = \int_{\frac{\xi_i - \beta_i}{\Delta_i}}^{\frac{\xi_i - \alpha_i}{\Delta_i}} \zeta_i^k G(\zeta_i, \xi_i)\, d\zeta_i. \tag{B3}$$

Substituting (B2) into (B1) gives

$$\begin{aligned} \frac{\partial \bar{\psi}}{\partial x_k}(\mathbf{x}) = \sum_{j=1}^{3} \frac{\partial f_j}{\partial x_k}(\mathbf{x}) & \left(\prod_{i \neq j} \sum_{k_i=0}^{+\infty} \frac{(-1)^{k_i}}{k_i!} \Delta_i^{k_i} M_i^{k_i}(\xi_i) D_{\xi_i}^{k_i} \right) \\ & \times \left(\sum_{k_j=0}^{+\infty} \frac{(-1)^{k_j}}{k_j!} \Delta_j^{k_j} \left(\frac{dM_j^{k_j}}{d\xi_j}(\xi_j) D_{\xi_j}^{k_j} + M_j^{k_j}(\xi_j) D_{\xi_j}^{k_j+1} \right) \right) \phi(\boldsymbol{\xi}), \end{aligned} \tag{B4}$$

where the two terms in parentheses appear owing to the fact that a derivative in one spatial direction affects only the filtering operation in this direction (terms in second parentheses) and leaves the filtering operations in other two directions intact (terms in first parentheses). Applying the filtering operation (20) to $\partial\psi/\partial x_k$, using the fact that

$$\frac{\partial \psi}{\partial x_k}(\mathbf{x}) = \sum_{j=1}^{3} \frac{\partial \phi}{\partial \xi_j}(\boldsymbol{\xi}) \frac{\partial f_j}{\partial x_k}(\mathbf{x}), \tag{B5}$$

and changing the order of summation and integration, the following equation is obtained:

$$\overline{\frac{\partial \psi}{\partial x_k}}(\mathbf{x}) = \sum_{j=1}^{3} \oint_{\mathbf{D}} \prod_{i=1}^{3} \frac{1}{\Delta_i} G\left(\frac{\xi_i - \eta_i}{\Delta_i}, \xi_i\right) \frac{\partial f_j}{\partial x_k}(\mathbf{y}) \frac{\partial \phi}{\partial \eta_j}(\boldsymbol{\eta})\, d^3\boldsymbol{\eta}. \tag{B6}$$

Introducing the change of variables $\eta_i = \xi_i - \Delta_i \zeta_i$ and performing the formal Taylor series expansion in powers of Δ_i we obtain

$$\frac{\partial f_j}{\partial x_k}(\mathbf{y}) = \sum_{l=0}^{+\infty} \frac{1}{l!} \left(\sum_{m=1}^{3} \sum_{k=1}^{+\infty} \frac{(-1)^k}{k!} \left(\sum_{i=1}^{3} \Delta_i \zeta_i D_{\xi_i} \right)^k F_m(\boldsymbol{\xi}) D_{x_m} \right)^l D_{x_k} f_j(\mathbf{x}), \tag{B7}$$

$$\frac{\partial \phi}{\partial \eta_j}(\boldsymbol{\eta}) = \sum_{k=0}^{+\infty} \frac{(-1)^k}{k!} \left(\sum_{i=1}^{3} \Delta_i \zeta_i D_{\xi_i} \right)^k D_{\xi_j} \phi(\xi). \tag{B8}$$

Once again, without loss of generality, we assume that radii of convergence of the above series are infinite. Note that Eqs. (B7)–(B8) are the three-dimensional analogs of Eqs. (13)–(14). Substituting (B7)–(B8) into (B6), using a procedure analogous to (19) and (B2), and combining terms of the same order we obtain

$$\begin{aligned} \left[\frac{\partial \psi}{\partial x_k} \right] = \sum_{i=0}^{+\infty} \sum_{j=0}^{+\infty} \sum_{l=0}^{+\infty} \Bigg(& A_{ijl} M_1^i(\xi_1) M_2^j(\xi_2) M_3^l(\xi_3) \\ & + \sum_{m=0}^{3} B_{ijl}^m \frac{d}{d\xi_m} M_1^i(\xi_1) M_2^j(\xi_2) M_3^l(\xi_3) \Bigg) \Delta_1^i \Delta_2^j \Delta_3^l, \end{aligned} \tag{B9}$$

where A_{ijl} and B_{ijl}^m $(i, j, l \geq 0,\ m = 1, 2, 3)$ are, in general, nonzero coefficients with the exception of A_{000}, which is always zero. Using the fact that $A_{000} = 0$, $M_i^k(\xi_i) = 0$ for $k = 1, \ldots, n-1$, and property (17) we obtain for the commutation error given by (21).

APPENDIX C

In this appendix we give the mathematical details of the minimization procedure described in Section III, which is used for constructing discrete filters with desired properties. The procedure consists in specifying a target filter function $\hat{G}_t(k)$ in wave number space and minimizing the difference between it and the Fourier transform of the discrete filter.

Without loss of generality let us consider the case of uniform grid with $\Delta = 1$. Then the Fourier transform $\hat{G}(k)$ of the discrete filter is given by (27). Without loss of generality Eq. (27) can be rewritten by omitting index j associated with the location of the filter. Then we have

$$\hat{G}(k) = \sum_{l=-K}^{L} \mathrm{w}_l\, e^{-ikl}. \tag{C1}$$

Let $N = K + L + 1$ be the total number of degrees of freedom; L_l is the total number of liner constraints which include both (26) and (30) constraints, $L_r = N - L_l$ is the number

of remaining degrees of freedom. Then the filter weights are given by

$$\mathrm{w}_l = \mathrm{w}_l^0 + \sum_{l=1}^{L_r} A_{lm} z_m, \tag{C2}$$

where z_m are real coefficients for the remaining degrees of freedom and A_{lm} is real $N \times L_r$ influence matrix. In the case when z_k are chosen to be one of the filter weights, the appropriate w_l^0 will be zero. Substituting (C2) into (C1) we obtain

$$\hat{G}(k) = \hat{G}_0(k) + \sum_{m=1}^{L_r} \left(\sum_{l=-K}^{L} A_{lm}\, e^{-ikl} \right) z_m = \hat{G}_0(k) + \sum_{m=1}^{L_r} (a_m(k) + i b_m(k)) z_m, \tag{C3}$$

where

$$a_m(k) = \sum_{l=-K}^{L} A_{lm} \cos(kl) \tag{C4}$$

and

$$b_m(k) = -\sum_{l=-K}^{L} A_{lm} \sin(kl). \tag{C5}$$

Let $\hat{G}_\mathrm{t}(k)$ be a target filter function, which we want $\hat{G}(k)$ to approach. Substituting (C3) into (31) we obtain the functional

$$\begin{aligned} \Phi(z_1, \ldots, z_{L_r}) = &\int_0^\pi \left(\sum_{m=1}^{L_r} a_m(k) z_m - \Re\{\hat{G}_\mathrm{t}(k) - \hat{G}_0(k)\} \right)^2 dk \\ &+ \int_0^\pi \left(\sum_{m=1}^{L_r} b_m(k) z_m - \Im\{\hat{G}_\mathrm{t}(k) - \hat{G}(k)\} \right)^2 dk. \end{aligned} \tag{C6}$$

Coefficients z_m can be chosen to minimize the functional $\Phi(z_1, \ldots, z_{L_r})$. It is easy to show that the minimum of the functional $\Phi(z_1, \ldots, z_{L_r})$ is obtained when z_m is the solution of the system of linear equations

$$\sum_{m=1}^{L_r} A_{lm} z_m = R_l, \tag{C7}$$

where A_{lm} is a positive definite $L_r \times L_r$ matrix given by

$$A_{lm} = \int_0^\pi (a_l(k) a_m(k) + b_l(k) b_m(k))\, dk \tag{C8}$$

and R_l is a vector given by

$$R_l = \int_0^\pi (a_l(k) \Re\{\hat{G}_\mathrm{t}(k) - \hat{G}_0(k)\} + b_l(k) \Im\{\hat{G}_\mathrm{t}(k) - \hat{G}(k)\})\, dk. \tag{C9}$$

ACKNOWLEDGMENT

This work was supported partially by the Office of Naval Research, Grant N00014-95-1-0221.

REFERENCES

1. S. Ghosal and P. Moin, The basic equations of the large eddy simulation of turbulent flows in complex geometry, *J. Comput. Phys.* **118**, 24 (1995).
2. H. van der Ven, A family of large eddy simulation (LES) filters with nonuniform filter widths, *Phys. Fluids* **7**, 1171 (1995).
3. A. Leonard, Energy cascade in large-eddy simulations of turbulent fluid flows, *Adv. Geophys.* **18**, 237 (1974).
4. T. S. Lund and H.-J. Kaltenbach, Experiments with explicit filtering for LES using a finite-difference method, in *Annual Research Briefs* (Center for Turbulence Research, NASA Ames/Stanford University, 1995), p. 91.
5. M. Germano, U. Piomelli, P. Moin, and W. H. Cabot, A dynamic subgrid-scale eddy viscosity model, *Phys. Fluids A* **3**, 1760 (1991).
6. S. Ghosal, T. S. Lund, P. Moin, and K. Akselvoll, A dynamic localization model for large-eddy simulation of turbulent flows, *J. Fluid Mech.* **286**, 229 (1995).
7. C. A. Kennedy and M. H. Carpenter, Several new numerical-methhods for compressible shear-layer simulations, *Appl. Numer. Math.* **14**, 397 (1994).
8. G. Beylkin, On the representation of operators in bases of compactly supported wavelets, *SIAM J. Numer. Anal.* **29**, 1716 (1992).
9. G. Beylkin and N. Saito, Wavelets, their autocorrelation functions, and multiresolution representation of signals, *Proc. SPIE* **LB26**, 39 (1993).
10. S. K. Lele, Compact finite difference schemes with spectral-like resolution, *J. Comput. Phys.* **103**, 16 (1992).